CHARGE SYMMETRY IN ^{13}N AND ^{13}C

A COUPLED-CHANNEL MODEL

Thesis by

George Fox

In Partial Fulfillment of the Requirements

for the Degree of

Doctor of Philosophy

California Institute of Technology

Pasadena, California

1979

(Submitted May 11, 1979)

ACKNOWLEDGEMENT

This thesis is dedicated to my wife Karen for her love and patience.

ABSTRACT

A set of coupled-channel differential equations based on a rotationally distorted optical potential is used to calculate the wave functions required to evaluate the gamma ray transition rate from the first excited state to the ground state in ^{13}C and ^{13}N. The bremsstrahlung differential cross section of low energy protons is also calculated and compared with existing data. The marked similarity between the potentials determined at each resonance level in both nuclei supports the hypothesis of the charge symmetry of nuclear forces by explaining the deviation of the ratios of the experimental E1 transition strengths from unity.

TABLE OF CONTENTS

I. INTRODUCTION

As a consequence of the charge symmetry of nuclear forces, corresponding E1 transitions in conjugate nuclei are expected to have equal strengths [Warburton and Weneser[1] and references therein]. Recent data compilations[2-4] for nuclei with A = 15-43 reveal that at present the absolute strengths of 18 pairs of such E1 transitions are available for comparison. The ratios of these E1 strengths in conjugate nuclei (fig. 1) deviate from equality by appreciable factors - in apparent disagreement with the charge symmetry hypothesis. This conclusion must, however, be relaxed since the E1 transitions in all of these nuclei are rather weak (E1 ~ 10^{-3} to 10^{-6} W.u.), and strong cancellations may be taking place in the matrix elements.[5] The largest deviation has been found[1,2] in the A = 15 system (factor ≥ 160, fig. 1) but here the E1 strengths are very small (E1 ~ 10^{-6} W.u.).

Such big differences in corresponding E1 transitions should, however, be less likely if the E1 strengths are large, as in the case of the A = 13 system. The E1 transition from the first excited state in ^{13}C [Γ_γ = 0.44 ± 0.05 eV; ref. 6] and ^{13}N [Γ_γ = 0.64 ± 0.07 eV; weighted average of refs. 7-10] have exceptionally large strengths of 0.04 and 0.13 W.u., respectively. Thus, the observed strength ratio of 3.2 ± 0.7 for these E1 transitions represents a more serious challenge to the charge symmetry concept. The subject of the present work is a theoretical investigation of this discrepancy in the A = 13 mirror system.

The El transition rule quoted above is exact in the long-wavelength approximation due to the vanishing of the isoscalar matrix element.[1] The next correction term in the isoscalar matrix element is of the order $(kr)^2$, and hence the contribution to an isoscalar radiative width from this term relative to a normal isovector radiative width will be of the order[1] $(kr)^4 \simeq 3 \times 10^{-6}$ for $E_\gamma = 3$ MeV and a nuclear radius of 2.8 fm. This correction term is much too small to explain the observed discrepancy.

The neutron-proton mass difference as well as the Coulomb forces will cause isospin mixing of the predominantly $T = 1/2$ low-lying states with $T = 3/2$ states at excitation energies[11] $E_x \gtrsim 15$ MeV. In the isobaric spin representation, the mixed states can be described[12]:

$$|\Psi_{low}\rangle = \alpha \mid T = \tfrac{1}{2}\rangle + \beta \mid T = 3/2\rangle$$

and

$$|\Psi_{high}\rangle = \beta \mid T = \tfrac{1}{2}\rangle - \alpha \mid T = 3/2\rangle$$

with $\alpha^2 + \beta^2 = 1$. If the Hamiltonian is written as a charge-independent (isospin-conserving) part H_o plus a charge-dependent part H_c, then the isospin-mixing element $M = \langle T = 3/2 | H_c | T = \tfrac{1}{2}\rangle$ is related to the coefficients α and β and to the observed difference D in the excitation energies of the two isospin states by the expression $M = \alpha\beta D$. For $D \sim 15$ MeV and a conservative value[12] of $M \lesssim 200$ keV, the product of the two coefficients is $\alpha\beta \sim 10^{-2}$. Since the low-lying states have a predominantly $T = \tfrac{1}{2}$ isospin (i.e., $\alpha \simeq 1$), one obtains a mixing coefficient $\beta \sim 10^{-2}$ as an order of magnitude estimate. This coefficient together with an assumed large intrinsic El-matrix element

of 1 W.u. for the T = $3/2^-$ state to ground state decay leads to a contribution of 10^{-4} W.u. in the E1 decay of the first excited state. The contribution is still 2-3 orders of magnitude too small when compared with the observed strengths and hence cannot contribute significantly to the explanation of the discrepancy. However, for the A = 15-43 nuclei this contribution is of the same order as the observed strengths and hence can play a significant role in their E1-transitions.

We have found that a sizable component corresponding to a nucleon coupled to the zero isospin first excited state of ^{12}C in the wave functions of both the ground and first excited states of ^{13}C and ^{13}N appears to be responsible for the difference in the mirror E1 strengths In the transition amplitude, this component in each of the levels interferes destructively with the component associated with the ^{12}C ground state. The resulting effect is to reduce the value of the ^{13}C width and in the ^{13}N cross section to lower the high energy tail of the resonance.

As a further test of the model, we have calculated the bremsstrahlung differential cross section for protons on ^{12}C up to a beam energy of 2 MeV in the laboratory system at $\theta_\gamma = 0^\circ$ and 90°. In this case we find that the reaction proceeds through a resonance in ^{13}N which interferes with the incoming distorted wave in the transition to the first excited state of ^{13}N. This resonance with energy 1.565 MeV in the center of mass and total spin, parity $J^\pi = 3/2^-$ can be described as consisting mainly of a proton coupled to the first excited state of ^{12}C because the $P_{3/2}$ shell if filled in $^{12}C(gs)$; thus, in the shell model, one cannot add another $P_{3/2}$ nucleon to $^{12}C(gs)$. This results in the narrow

resonance observed in the differential cross section at $\theta = 0°$. A second resonance at 6.976 MeV with $J^\pi = 1/2^-$ aids in modeling the incoming wave and in conjunction with the previous resonance, the differential cross sections at $\theta = 0°$ and $\theta = 90°$.

Section II presents the standard deformed spherical potential coupled-channel model. In addition, this section deals with the normalization problems that arise in defining spectroscopic factors. Section III outlines the changes in gamma ray matrix elements needed to compute transitions with multiple input spins and channels. Also included is a solution to the problem of computing the matrix elements between free (continuum) particle states. Section IV applies these ideas to understanding charge symmetry in mass 13 by computing the capture and bremsstrahlung cross sections. Section V is a discussion and interpretation of the models presented above with suggestions for further study. The Appendix contains all the relevant information for creating and running the program on a high speed digital computer.

II. THE COUPLED-CHANNEL EQUATIONS

A. The Rotational and Vibrational Models

Starting from an optical model potential of the Woods-Saxon form, Tamura[14] derives the form of the off-diagonal potentials when specific assumptions are made concerning the shape of the nuclear surface. The point of view taken is that the nuclear potential is directly proportional to the mass distribution within the core. Thus we can expand the radius of the nuclear surface into any form which allows easy insertion into the optical potential and subsequent expansion to accommodate coupled channel modes. The usual models employed are the vibrational model which expands the radius in a full set of spherical harmonics and the rotational model which assumes an axially symmetric deformed nucleus expansion. It is usual to neglect the higher order expansions of the spin-orbit potential and keep only the spherical term. In the discussion of Section V a brief analysis of the spin-orbit potential and its origin will be presented in an attempt to illuminate the proper procedure to follow. Similarly, for the Coulomb potential we have only included diagonal terms, as the off-diagonal terms are much smaller than the corresponding nuclear off-diagonal terms. We first consider the total Hamiltonian,

II.1
$$H = T + H_t + V(\vec{r}, \vec{\xi})$$

where T is the kinetic energy of the projectile, H_t is the target Hamiltonian, and $V(\vec{r}, \vec{\xi})$ is a generalized potential describing the

interaction of the target with the projectile. The target Hamiltonian

has Schroedinger equation solutions $\Phi_{I_n M_n}$ given by

II.2
$$H_t \, \Phi_{I_n M_n} = \omega_n \, \Phi_{I_n M_n}$$

where I_n, M_n are the core spin and its projection and ω_n is the energy of

the core state. One now writes the total wave function,

II.3
$$\Psi = r^{-1} \sum_{J n \ell_n j_n} R_{J n \ell_n j_n}(r) \, (\mathcal{Y}_{\ell_n j_n} \otimes \Phi_{I_n})_{JM}$$

$$(\mathcal{Y}_{\ell_n j_n} \otimes \Phi_{I_n})_{JM} = \sum_{m_j M_n} (j_n I_n m_j M_n | JM) \mathcal{Y}_{\ell_n j_n m_j} \, \Phi_{I_n M_n}$$

$$\mathcal{Y}_{\ell_n j_n m_j} = \sum_{m_\ell m_s} (\ell s m_\ell m_s | j m_j) i^\ell \, Y_{\ell_n m_\ell} \, X_{s m_s}$$

where $X_{s m_s}$ is the spin wave function of the projectile, $R_{J n \ell_n j_n}(r)$ is

the radial wave function of the projectile with total spin and

projection J,M, formed from coupling core spin I_n and projectile total

spin j_n. The total projectile spin j_n is formed from orbital angular

momentum ℓ_n and the particle intrinsic spin.

To get the coupled-channel equations we now insert the total wave

function Ψ into the full Schroedinger equation, multiply on the left by

$(\mathcal{Y}_{\ell_n j_n} \otimes \Phi_{I_n})^*_{JM}$ and integrate over all variables except r to obtain

II.4 $(\frac{\hbar^2}{2m} \frac{d^2}{dr^2} - \frac{\hbar^2}{2m} \frac{\ell_n(\ell_n+1)}{r^2} + E_n) \, R_{Jn\ell_n j_n}(r) =$

$$\sum_{n'\ell_n' j_n'} < (Y_{\ell_n' j_n'} \otimes \Phi_{I_n'})_{JM} |V| (Y_{\ell_n j_n} \otimes \Phi_{I_n})_{JM} >$$

$$R_{Jn'\ell_n' j_n'}(r)$$

where $E_n = E_1 - \omega_n$, and the matrix element is over all variables except r. The crux of the problem is now reflected in the evaluation of the matrix elements of the generalized potential.

In general we can expand the potential as

II.5 $$V = \sum_{\lambda,t} \nu_\lambda^{(t)}(r) \, (Q_\lambda^{(t)} \cdot Y_\lambda)$$

where the subscript λ denotes the potential of tenor rank λ and the superscript t distinguishes terms of different character. Y_λ is an angular momentum function of the projectile's angular variables and $Q_\lambda^{(t)}$ operates only on the coordinates of the core. A calculation of the above matrix element yields

II.6 $<\ell j I |V| \ell'j'I'> =$

$$\sum_{t,\lambda} \nu_\lambda^{(t)} <I|| Q_\lambda^{(t)} || I'> A(\ell j I, \ell'j'I';\lambda J s)$$

where $A(\ell j I, \ell'j'I';\lambda J s)$ is a completely geometrical factor given by

II.·7 $A(\ell jI,\ell'j'I';\lambda Js) = (4\pi)^{-\frac{1}{2}}(-)^{J-s-I'+\ell+\ell'+\frac{1}{2}}(\ell'-\ell)(2\ell+1)^{\frac{1}{2}}(2\ell'+1)^{\frac{1}{2}}$

$\qquad (2j+1)^{\frac{1}{2}}(2j'+1)^{\frac{1}{2}}(\ell\ell'oo|\lambda o)W(jIj'I';J\lambda)W(\ell j\ell'j';s\lambda)$

and the reduced matrix element is defined as

II.8 $<IM_I|Q^{(t)}_{\lambda\mu}|I'M_I,>=<I\| Q^{(t)}_\lambda\| I'> (2I+1)^{-\frac{1}{2}}(I'\lambda M_I'\mu|IM_I).$

In the rotational model the nuclear surface is expanded as

II.9 $R = R_o(1 + \sum_\lambda \beta_\lambda Y_{\lambda o}(\theta')),$

where $R_o = r_o A^{1/3}$ is the usual optical model radius formula, $r_o=1.25fm$, the
angle θ' refers to the body fixed system. This deformed radius parameter
is now inserted into the Woods-Saxon potential shape and the potential is
expanded in spherical harmonics,

II.10 $V = \sum_{\lambda\mu} \nu_\lambda(r) D^\lambda_{\mu o}(\theta_i)Y_{\lambda\mu}(\theta,\phi)$

$\qquad \nu_\lambda = 2\pi \int^{+1}_{-1} V(R_o(1+ \sum_\lambda \beta_\lambda Y_{\lambda'o}(\theta')))Y_{\lambda o}(\theta')d(\cos \theta')$

where $D^\lambda_{\mu o}$ is a rotation from the space fixed to the body fixed
coordinates,

$\qquad Y_{\lambda o}(\theta') = \sum_\mu D^\lambda_{\mu o}(\theta_i) Y_{\lambda\mu}(\theta,\phi)$

For the vibrational model the optical potential radius is expanded
in a full set of spherical harmonics,

II.11 $R = R_o(1 + \sum_{\lambda\mu} \alpha_{\lambda\mu} Y_{\lambda\mu}(\theta,\phi))$

and a procedure similar to the rotational model is followed to obtain the tensor potential expansion.

C.   IDENTICAL PARTICLES AND SPECTROSCOPIC FACTORS

There are counting and timing problems which arise when treating systems of many particles in real time. The single particle stationary state Schroedinger equation when used in a multiparticle, real time evolution process must be corrected for two phenomena. Some particles in the system can interact quite strongly within the time limits governing a particular process, while others may remain inert and noninteracting. For example, in discussing single particle gamma ray transitions which occur in outer shells, as long as the time for the core to interact with the extra particles is long compared with transition lifetime, the core can be considered to be inert and will enter into the process in only the most simple ways. Second, charge can be exchanged in the strong interactions between nucleons and hence all particles within a shell, regardless of charge, must be included in computing spectroscopic factors.

The statistics and configurations of the mass 13 states of interest will now be described so that some insight can be gained in understanding the results of section IV. The ^{4}He core consisting of two protons and two neutrons in the 1s-shell is very stable; its first excited state does not occur until nearly 20 MeV. Hence, in all that follows its only contribution is to mass and charge. In the ^{12}C ground state the next

eight particles are all in ℓ=1 states and are considered to form a semi-magic shell since they fill up the total angular momentum states j=3/2 obtained by coupling spin and orbital angular momentum in parallel. In constructing the mass 13 ground state the extra nucleon is put into the next ℓ=1 level which has j=1/2, antiparallel spin and orbital angular momentum. In this case however the excitation of the core mixes up the distinction between parallel and antiparallel spin and angular momentum, with the consequence that all p-shell nucleons are treated the same,giving a total spectroscopic factor of 9. Similar reasoning can be applied to the other bound states in the compound nucleus. For all particle unbound channels the wave functions have been normalized to unit incoming flux.

III. GAMMA RAY TRANSITIONS

A. TRANSITION PROBABILITIES FOR MULTIPLE CHANNELS

The procedure which we outline here is presented in more detail by Johnson[15] and is a modification of the Rose and Brink[16] formulas for the angular distributions of gamma rays. The changes are a result of using more than one total spin state in the incident channel.

The differential cross section for a photon of wave number $\vec{k}_\gamma$ in the direction θ is given by $\rho(\vec{k}_\gamma)$, the probability of emission in the direction θ divided by the incident particle velocity. These probabilities in turn can be written as being proportional to the absolute squares of amplitudes given by

$$\text{III.1} \qquad A^q_{M_1 M_2}(\vec{k}_\gamma) \sim \sum_{L,M,\pi} q^\pi \langle J_1 M_1 | T^{<\pi>}_{LM} | J_2 M_2 \rangle \, \mathcal{D}^L_{Mq}(R)$$

where q is the polarization of the radiation and $T^{<\pi>}_{LM}$ is the interaction multipole operator of type L,π and $\mathcal{D}^L_{Mq}(R)$ is a rotation operator where the rotation R takes the z-axis to $\vec{k}_\gamma$.

These amplitudes are simply summed over the possible total spin angular momentum states in the initial channel and the absolute value is squared to obtain the probability. By using the Wigner-Echart theorem and the reduction formula for a product of rotation matrices plus the usual Clebsch-Gordan and Racah algebra, we arrive at the angular distribution for photons of polarization q from states J_1 and J_1' leading to a state J_2.

III.2 $\qquad P^q(\vec{k}_\gamma) = (k_\gamma/2\pi h) \sum_{KLL'\pi\pi'} B_K(J_1) P_K(\cos\theta)(-)^{q+J_1-J_2+L'-L-K'}$

$$\cdot (LL'q-q|KO)\ W(J_1J_1'LL';KJ_2)$$

$$\cdot q^{\pi+\pi'} <J_1\| T_L^{<\pi>} \| J_2><J_1'\| T_{L'}^{<\pi'>} \| J_2>^*$$

where $B_K(J_1,J_1') = \sum_{M_1} w(M_1)(-)^{J_1-M_1} (2J_1+1)^{\frac{1}{2}}(2J_1'+1)^{\frac{1}{2}}(J_1J_1'M_1-M_1|KO)$

$\qquad B_0(J_1,J_1') = 0\ ,\ \sum_{M_1} w(M_1) = 1,$

where $w(M_1)$ is the incoming probability distributions over total angular momentum projections. The appendix contains the formulas used for the computations in a much more reduced form.

B.   FREE PARTICLE MATRIX ELEMENTS

The r^λ matrix element between free particle initial and final states can be evaluated using standard techniques from complex functional analysis.[13] For the free particle wave functions we use an integral representation of an outgoing Coulomb wave. (With simple changes in parameters, the matrix elements of zero charge and bound state wave functions can also be obtained.) The outgoing Coulomb wave is written in a way which illustrates its asymptotic form,

III.3 $\qquad O_L(\eta,\rho) = G_L(\eta,\rho) + i\ F_L(\eta,\rho) = e^{i\theta_L(\eta,\rho)} \dfrac{\int_0^\infty dt\ e^{-t} t^{L+i\eta}(1+it/2\rho)^{L-i\eta}}{\Gamma(L+i\eta+1)}$

where $\qquad \theta_L(\eta,\rho) = \rho-\eta \log(2\rho) - L\dfrac{\pi}{2} + \sigma_L$

$\qquad \sigma_L = \arg \Gamma(L+1+i\eta)$

$$\rho = kr$$

and L, k, η are the usual angular momentum, wave number, and dimensionless Coulomb potential strength, respectively. To evaluate the truncated matrix element (that is, the integral from a finite radius to infinity), the r-dependent terms are grouped together after a direct substitution.

III.4
$$<O_{L_i}|r^\lambda|O_{L_f}>_R = \int_R^\infty dr\, O_{L_i}^*(\eta_i,k_i r)r^\lambda\, O_{L_f}(\eta_f,k_f r)$$

$$= e^{i(\eta_i \log 2k_i - \eta_f \ln 2k_f + (L_i - L_f)\frac{\pi}{2} + \sigma_f - \sigma_i)}\int_R^\infty dr\, r^{\lambda + L_i + L_f + 2}$$

$$\cdot\, e^{-(i(k_i - k_f) + u + t)r}$$

$$\frac{\int_0^\infty dt\, t^{L_i - i\eta_i}(1 - it/2k_i)^{L_i + i\eta_i}}{\Gamma(L_i - i\eta_i + 1)} \quad \frac{\int_0^\infty du\, u^{L_f + i\eta_f}(1 + iu/2k_f)^{L_f - i\eta_f}}{\Gamma(L_f + i\eta_f + 1)}$$

After performing the integral over r, a change of variables $(t = i\rho_{if}sx,\ u = i\rho_{if}s(1-x))$ and a contour integral whose validity is justified by Cauchy's integral theorem and analytic continuation, we get

III.5
$$<O_{L_i}|r^\lambda|O_{L_f}>_R = e^{i(\theta_{L_f}(\eta_f,k_f R) - \theta_{L_i}(\eta_i,k_i R))}R^{\lambda + 1}\sum_{L=0}^{L}\frac{L!}{(L-L)!}I_{L+1}$$

where

$$I_{L+1} = (i\rho_{if})^{a - (L+1)}\int_0^\infty ds\, e^{-i\rho_{if}s}\frac{s^{a-1}}{(1+s)^{L+1}}(1 + \frac{xs\rho_{if}}{2\rho_i})^{L_i + i\eta_i}$$

$$\cdot\, (1 - \frac{(1-x)s\rho_{if}}{2\rho_f})^{L_f - i\eta_f}$$

$$\int_0^1 dx\, \frac{x^{L_i - i\eta_i}(1-x)^{L_f + i\eta_f}}{\Gamma(L_i - i\eta_i + 1)\Gamma(L_f + i\eta_f + 1)}$$

$$L = \lambda + L_i + L_f + 2$$

$$a = L_f + L_i + 2 + i(\eta_f - \eta_i)$$

$$\rho_i = k_i R, \qquad \rho_{if} = \rho_i - \rho_f$$

This last double integral can now be approximated by an asymptotic series in confluent hypergeometric functions after first expanding the two terms in the numerator.

$$\text{III.6} \qquad I_{L+1} = \sum_{N=0}^{\infty} N! \; i^N \, C_N(\rho_i, \rho_f)(i\rho_{if})^{b-1} \, U(a,b,i\rho_{if})$$

where $\quad b = a - L$

$$C_N(\rho_i, \rho_f) = \sum_{\substack{\ell=0 \\ j=N-\ell}}^{N} \left\{ \frac{\Gamma(L_i+i\eta_i+1)}{\ell! \, \Gamma(L_i-\ell+i\eta_i+1)} \right\} \left\{ \frac{\Gamma(L_i-i\eta_i+\ell+1)}{\ell! \, \Gamma(L_i-i\eta_i+1)} \right\} \left\{ \frac{\Gamma(L_f-i\eta_f+1)}{j! \, \Gamma(L_f-j-i\eta_f+1)} \right\}$$

$$\cdot \left\{ \frac{\Gamma(L_f+i\eta_f+j+1)}{j! \, \Gamma(L_f+i\eta_f+1)} \right\} \frac{\ell! \, j!}{N!} \left(-\frac{1}{2\rho_i}\right)^{\ell} \left(\frac{1}{2\rho_f}\right)^{j}$$

$U(a,b,z)$ is defined in Abramowitz and Stegun[17] (13.1.3).

The full (R=0) matrix element is obtained in a more straightforward manner by first expanding the two numerator terms as before. The integrals then reduce to nothing more than sums and products of Γ-functions. This final series is

$$\text{III.7} \qquad \langle 0_{L_i}|r^{\lambda}|0_{L_f}\rangle = \frac{(2k_i)^{i\eta_i}}{(2k_f)^{i\eta_f}} \, e^{i\frac{\pi}{2}(L_i-L_f)} e^{i(\sigma_f-\sigma_i)}$$

$$\Gamma(\lambda+1+i(\eta_f-\eta_i))\left(\frac{k_i-k_f}{i}\right)^{-(\lambda+1+i(\eta_f-\eta_i))}$$

$$\sum_{N=0}^{\infty} \left\{ \frac{N! \, \Gamma(\lambda-N+1(i(\eta_f-\eta_i)))}{\Gamma(\lambda+1+i(\eta_f-\eta_i))} \right\} C_N(k_i,k_f) \, k_{if}^N$$

IV. APPLICATION TO GAMMA TRANSITIONS IN MASS 13

Figure 2 shows a nuclear energy level isobar diagram for mass 13. We will be concerned with modeling the structure of these low-lying states.

Mikoshiba, et al.[19], find that an axially symmetric, rotational nucleus with large oblate deformation successfully reproduces the experimental phase shifts, cross sections, and polarizations of elastic scattering of nucleons on ^{12}C whereas the vibrational model cannot. The doctoral dissertation of Johnson[15] extends the model to include nucleon capture on ^{12}C.

Neither effort is successful at low energies as a result of problems in combining in a consistent fashion bound and unbound channels within the same total wave function. The rotational model will be used to calculate wave functions for these low energy states and the resulting E1 transition rates between them in an attempt to illuminate some of these inconsistencies.

The E1 strengths for the transition from the first excited $J^{\pi}=\frac{1}{2}^{+}$ state to the $J^{\pi}=\frac{1}{2}^{-}$ ground state in each nuclei will be predicted and ratio compared to the experimental value. We will find that the computed ratio agrees quite well with the experimental ratio; hence, for this transition we find no violation of the charge symmetry of nuclear forces. In addition the bremsstrahlung radiation from protons on ^{12}C will be modeled as occurring through one resonance - the $J^{\pi}=3/2^{-}$ state at 3.509 MeV - and the incoming plane wave modeled as the higher

$J^\pi=\frac{1}{2}^-$ state at 8.92 MeV – to the $J^\pi=\frac{1}{2}^+$ first excited state at 2.366 MeV.

From the calculations of Cohen and Kurath[18] for single nucleon transfer reactions in the 1p-shell, we obtain spectroscopic factors for the two most important low-lying contributions to the mass 13 ground state.

IV.1 $\quad |gs> = \theta(0^+)|^{12}C(g.s.)$ + nucleon> $\theta(2^+)|^{12}C(2^+)$ + nucleon>

where $\theta(0^+)$ and $\theta(2^+)$ are the fractional parentage coefficients. The spectroscopic factors are given by the square of the fractional parentage coefficients times the number of extra core nucleons as explained in Section II B. Cohen and Kurath determine the spectroscopic factors,

$$S(0^+) = 0.6132 \quad \text{and} \quad S(2^+) = 1.1218$$

In coupling the $^{12}C(g.s.)$ and $^{12}C(2^+)$ with single particles to form the ^{13}C and ^{13}N ground states we proceed as follows. The strength of the off-diagonal mixing potential is calculated using the rotational coupled-channel model. The diagonal nuclear optical potentials in each channel are forced to be equal and this strength and that of the spin-orbit potential are varied to put each ground state at the proper eigenenergy with the correct spectroscopic factors. These wave functions are then used in the computation of the El matrix elements in conjunction with the first excited state wave functions. Variations of the diagonal and spin-orbit potential strengths for the first excited state result in the reproduction of the $^{12}C(p,\gamma)^{13}N$ capture cross

section (Figure 4) by estimating its value at the resonance energy and at proton energy .700 MeV (center of mass). The resulting normalization factor gives the ground state (0^+ and 2^+ states only) spectroscopic factor since the $J^\pi = 1/2^+$ state is normalized to unit incoming flux. From this computation we also obtain estimates of the $^{12}C(p,p)^{12}C$ S-wave phase shifts[20] which are excellent over the entire energy region of interest (Figure 3)

Potential strengths identical to those used for the mixing and spin-orbit potentials in ^{13}N, are then applied in computing the ^{13}C ground and first excited states. Again, the diagonal potential is varied to put the wave functions at the right eigenenergies. The El transition width is computed and multiplied by the ground state spectroscopic factor estimated in the ^{13}N computation. From the capture cross section in ^{13}N a simple computation yields its gamma width. The peak is modeled as a Breit-Wigner form and the gamma width is computed assuming that the proton width is approximately equal to the full width.

In performing the bremsstrahlung calculation a similar procedure is followed. The $J^\pi = 1/2^+$ excited state potential values computed in the previous calculation are used to generate what will be the final state wave functions in this problem. Using the mixing potential values predicted by the rotational model we then construct the $J^\pi = 3/2^-$ and $J^\pi = 1/2^-$ excited states. The $J^\pi = 1/2^-$ state is used only to simulate

the $P_{\frac{1}{2}}$ piece of the incoming plane wave. The $J^{\pi}=3/2^{-}$ potential values are then varied to arrive at the best fit to the $\theta = 0^{\circ}$ bremsstrahlung cross section, using the El bremsstrahlung differential cross section formula from Appendix B. A factor for the final state phase space density and a simple integral of the Breit-Wigner resonance shape for the $J^{\pi}=1/2^{+}$ final state were also included. The $\theta = 90^{\circ}$ cross section was also determined, and is the dotted line of Figure 6. As can be seen from the figure the fit is qualitatively correct but missed some data badly. An examination of the experimental photon line shapes reveals the reasons for the problem. The background fluctuations at low energies are quite large, typically ten to fifteen percent of the resonance peak values, and secondly, the line shapes deviate quite severely from a Breit-Wigner form. To correct this problem we have computed the line shapes over the final state resonance region for selected values of the incident proton energy. The areas of the resulting peaks are numerically computed after lower limits to the peaks are inserted. Figure 7 shows a set of these peaks for a range of incident proton energies. The resulting final cross sections can be seen as the solid line in Figure 6 for $\theta = 90^{\circ}$. The lower limits to the peaks were determined using two rules of thumb. First, the line shapes should look closely like a Breit-Wigner resonance, hence the asymmetry of the peaks reduces the area. Second, the background noise results in making the placement of lower limits uncertain. The experimental line shapes had lower limits less than three half widths

wide. Even assuming a pure Breit-Wigner form for the peak, cutting off the base at three half widths yields a large reduction in area. The solid line of Figure 6 shows quite vividly the large changes to the 90° differential cross section.

Again the ^{13}N potential strengths are applied to the ^{13}C mirror transition states and the equivalent gamma widths are computed. Table 1 contains a listing of these widths for the $J^{\pi}=1/2^{+}$ state transition to the $J^{\pi}=1/2^{-}$ ground state and the $J^{\pi}=3/2^{-}$ state transition to $J^{\pi}=1/2^{+}$ state in both nuclei as well as a comparison with the experimental values. Table 2 contains a listing of the potential values for all states corresponding to the widths computed in Table 1.

It should be noted that the infrared divergence in the bremsstrahlung cross section seen at low energies as the dashed curve in Figure 6 is a result of the breakdown of perturbation theory for small photon energies. The perturbation term is a linear approximation to the matrix element of a complex valued exponential function of the perturbation potential between the initial and final states. Even though this linearized term goes to infinity for small photon energies as do all higher terms in the perturbation expansion, the exact term remains finite; higher order terms don't help the expansion converge. Summing the peaks as done here to correct the bremsstrahlung cross section also yields the added bonus of the disappearance of this divergence. As can be seen by examining Figure 7, as one goes to smaller photon energies the Breit-Wigner part of the peak grows smaller

even though the total area under the peaks goes to infinity.

V. DISCUSSION

A cursory examination of Table 2 reveals two significant features of the potential strength values. The first conclusion is that the spin-orbit strength varies quite widely across states. In performing the calculations the mixing potentials were fixed by the rotational model and we have truncated the full channel expansion to only two excited states of ^{12}C. Hence we shouldn't really expect any great consistency in the spin-orbit strength across states. The second major feature is the differences between the diagonal potentials in even and odd angular momentum states. The S and D shell potentials are approximately 54 MeV strong, whereas the P-waves are bound somewhat more weakly, approximately 42 MeV. One can only speculate as to the origin of this effect, but again the truncation of excited core states may play an important role.

In the standard derivation of the existence of the spin-orbit force a Dirac equation is derived from principles of relativistic invariance. The resulting spinor wave function is approximated by a scalar wave function with the Dirac equation being transformed from a coupled first order differential equation to a scalar second order Schroedinger equation with a spin-orbit potential and higher order terms. That is we've reduced a coupled wave function to a scalar wave function. For this reason it is probably correct not to distort the spin-orbit force; in fact the correct approach to deriving a coupled-channel model should start with a Dirac equation, the inclusion of core wave functions, and

a model of the excitation process. Such a procedure is beyond the scope of this paper.

As mentioned earlier, the failure of current models to adequately model the low energy states is most probably explained by the converse success of the models in consistently reproducing higher energy states. Conservation of energy and flux fix the amplitudes of all unbound channels whereas bound states can take on any normalization. Thus all that the standard models do at higher energies is determine the phase relationships between wave functions; at lower energies when bound states exist we must also mix in the proper amplitudes.

The resulting effects on matrix elements are unknown; it may be fruitful to pursue just what happens at these important thresholds. Further insight can also be obtained by examining the role of complex valued potentials. It is well known that the use of an imaginary valued potential results in the loss of flux from open channels because the Hamiltonian becomes non-Hermetian. Further investigation into the use of complex valued wave functions and potentials and their proper interpretations would be of invaluable help in unraveling the mysteries of the nucleus.

APPENDIX

A. Numerical Solution of Coupled Second Order Differential Equation System

    1. Solution by iteration of coupled equations

    2. Boundary conditions and solution search routines

    3. Computation of external matching functions

B. Gamma Ray Transition Differential Cross Section Formulas

C. Nuclear and Coulomb Potential Shapes

D. Computer Program Information

A. NUMERICAL SOLUTION OF SECOND ORDER COUPLED
DIFFERENTIAL EQUATION SYSTEM
1. SOLUTION BY ITERATION OF COUPLED EQUATIONS

The system of second order coupled differential equations is given by

$$(1) \qquad \frac{d^2\vec{y}}{dr^2} = A\vec{y}$$

where A is a matrix specified by the particular model used. Diagonal elements of A are the energy eigenvalues and central potentials of each channel. The off-diagonal elements are the mixing potentials. In the standard 3-point integration formula,

$$(2) \qquad \vec{y}_{n+1} = 2\vec{y}_n - \vec{y}_{n-1} + \frac{h^2}{12}(\vec{y}''_{n+1} + 10\vec{y}''_n + \vec{y}''_{n-1})$$

where h is the step size and $\vec{y}_n = \vec{y}(r=nh)$. We substitute (1) in for the second derivatives obtaining

$$(3) \qquad X_{n+1}\vec{y}_{n+1} = (12X_n^{-1} - 10)\, X_n\vec{y}_n - X_{n-1}\vec{y}_{n-1}$$

where $X_n = I - \frac{h^2}{12} A_n$. At the origin our starting conditions are $X_o\vec{y}_o = \vec{0}$, and at step 1 we arbitrarily set $X_1\vec{y}_1 = \vec{a}$ and define $X_{n+1}\vec{y}_{n+1} = Z_{n+1}\vec{a}$. After dropping $\vec{a}$ from all equations, we are left with a set of matrix equations to iterate,

$$(4) \qquad Z_{n+1} = (12X_n^{-1} - 10)\, Z_n - Z_{n-1}$$

with $Z_o = 0$, $Z_1 = I$.

We use equation set (4) when we search for the eigenvalue or resonance and equation set (3) when our desired solution is found. The usual error analysis and behavior is carried over from the one-dimensional case and can be found in Melkanoff, et al.[22]

2. BOUNDARY CONDITIONS AND SOLUTION SEARCH ROUTINES

For the case when all channels are bound, we must have only exponentially decreasing wave functions at infinity, the Whittacker function, and these are easily matched to the iterated solution in each channel. In all other cases we must have outgoing waves in at least one channel, so our outgoing wave function must behave asymptotically like

$$(5) \qquad \Psi_s \sim \frac{(4\pi)^{\frac{1}{2}}}{k_i} \left(e^{i\sigma_{\ell_i}} \delta_{is} F_{\ell_i} + C_s e^{i\sigma_{\ell_s}} (G_{\ell_s} + iF_{\ell_s}) \right)$$

where s is any channel, i is the incident channel, k_i the wave number in the incident channel, F_ℓ and G_ℓ are the regular and irregular Coulomb functions, respectively, but can be replaced by spherical Bessel functions in the case of no charge interactions; or if a channel is bound, $G_{\ell_s} + iF_{\ell_s}$ is replaced by a Whittaker function. C_s contains amplitude and phase shift information about the outgoing state. For the entrance channel $C_i = e^{i\delta} \sin \delta$ where δ is the commonly defined phase shift, and σ_{ℓ_s} is the Coulomb phase shift in channel s.

In the case where at least one channel is open, we integrate our system of equations starting from the origin so as not to introduce numerical errors from the irregular solution. The iterated wave

functions are matched to standard functions at two points for large
values of r. That is,

$$
(6) \qquad Z_\alpha a = \frac{(4\pi)^{\frac{1}{2}}}{k_i} \begin{bmatrix} e^{i\sigma_i} F_{\ell_i}(\alpha) + C_i \, e^{i\sigma_i}(G_{\ell_i}(\alpha) + iF_{\ell_i}(\alpha)) \\ \vdots \\ C_s \, e^{i\sigma_s}(G_{\ell_s}(\alpha) + iF_{\ell_s}(\alpha)) \\ \vdots \end{bmatrix}
$$

for $\alpha = 1, 2$, the functions all evaluated at the matching points. We can
write this in matrix notation and easily solve for the vectors $\vec{a}$ and $\vec{c} =$
$(\ldots, C_s, \ldots)$.

$$
(7) \qquad \begin{bmatrix} Z_1 & \mathrm{Diag}[e^{i\sigma_s}(G_{\ell_s}^1 + iF_{\ell_s}^1)] \\ & \\ Z_2 & \mathrm{Diag}[e^{i\sigma_s}(G_{\ell_s}^2 + iF_{\ell_s}^2)] \end{bmatrix} \begin{bmatrix} \vec{a} \\ \\ \frac{(4\pi)^{\frac{1}{2}}}{k_i}\vec{c} \end{bmatrix} = \frac{(4\pi)^{\frac{1}{2}}}{k_i} \begin{bmatrix} e^{i\sigma_i} F_{\ell_i}^1 \\ 0 \\ \vdots \\ 0 \\ e^{i\sigma_i} F_{\ell_i}^2 \\ 0 \\ \vdots \\ 0 \end{bmatrix}
$$

For the case where all channels are bound, we must integrate from
the ends toward the middle of the interval because of the numerical errors
introduced by the irregular solutions to the differential equations. From
the origin out we have the solution matrices Z_K', Z_{K+1}' and from infinity in
we have Z_K, Z_{K+1}. For arbitrary starting vectors $\vec{a}$ from the origin and
$\vec{b}$ from infinity we have the solutions at the points K and K+1,

$$
\vec{y}_K' = X_K^{-1} Z_K' \vec{a} \, , \qquad \vec{y}_{K+1}' = X_{K+1}^{-1} Z_{K+1}' \vec{a}
$$

(8) and

$$
\vec{y}_K = X_K^{-1} Z_K \vec{b} \, , \qquad \vec{y}_{K+1} = X_{K+1}^{-1} Z_{K+1} \vec{b}
$$

We have a proper solution to the differential equations when the values at each point are the same. This implies that we solve the matrix equation

$$
(9) \qquad A \begin{bmatrix} \vec{a} \\ \vec{b} \end{bmatrix} = \begin{bmatrix} Z'_K & -Z_K \\ \\ Z'_{K+1} & -Z_{K+1} \end{bmatrix} \begin{bmatrix} \vec{a} \\ \\ \vec{b} \end{bmatrix} = \vec{0}
$$

When the determinant of A is zero, then we have found a good solution to the system of equations. To find the starting vectors $\vec{a}$ and $\vec{b}$, simply set $a_1 = 1$ and solve the resulting system of equations.

3. COMPUTATION OF EXTERNAL MATCHING FUNCTIONS

The asymptotic values of the bound channel wave functions for both charged and uncharged states were computed using a 20-point Laguerre quadrature formula on the integral representation of the Whittaker function

$$
(10) \qquad W(\eta, \ell + \tfrac{1}{2}, 2\rho) = \frac{\exp(-\rho - \eta \, \ell n \, 2\rho)}{\Gamma(1 + \ell + \eta)} \int_0^\infty t^{\ell + \eta} e^{-t} (1 + t/2\rho)^{\ell - \eta} \, dt
$$

The nodes and weights are given by Stroud and Secrest[23]. The error in the quadrature can be limited to the boundedness of the fortieth derivative of the integrand times the error coefficient of 0.7254E-11. Representative values of these functions have been checked against tables in Abramowitz and Stegun[17].

The spherical Bessel functions are computed from formulas 10.1.2 in Abramowitz and Stegun[17]. The irregular solution can be recursed by

a three-point formula up in ℓ-values, starting being facilitated by the
analytic forms for $\ell=0$ and 1. The regular solutions are started
arbitrarily at high ℓ-values and recurred downward. The Wronskian is
then computed and used to correct the regular solutions. This routine
has also been checked against tables.

The Coulomb functions are computed by a program developed at the
University of Minnesota. Representative values have been checked against
tables in Abramowitz and Stegun[17] and Arnold Tubis, Tables of Nonrela-
tivistic Coulomb Wave Functions, Los Alamos Scientific Laboratory (1958).
The irregular Coulomb wave and its derivative for ℓ-values are obtained by
recursion. The regular solutions are obtained by a downward recursion
and these solutions are corrected by a Wronskian calculation.

B. GAMMA RAY TRANSITION DIFFERENTIAL CROSS SECTION FORMULA

The derivation of the formulas used in generating the cross sections of interest can be found in Johnson.[15]

For the E1-bremsstrahlung differential cross section, we obtain

$$(11) \quad \frac{d\sigma^{(\theta)}}{d\Omega} = \frac{k_\gamma}{6\pi\hbar v_i} [\{2|\langle \tfrac{1}{2}^- \| T_1^e \| \tfrac{1}{2}^+ \rangle|^2 + 4|\langle 3/\bar{2}|T_1^e \| \tfrac{1}{2}^+ \rangle|^2 \} P_o(\cos\theta)$$

$$+ \{4 \ \mathrm{Re}(\langle \tfrac{1}{2}^- \| T_1^e \| \tfrac{1}{2}^+ \rangle * \langle 3/2^- \| T_1^e \| \tfrac{1}{2}^+ \rangle$$

$$-2|\langle 3/2^- \| T_1^e \| \tfrac{1}{2}^+ \rangle|^2 \} \ P_2(\cos\theta)]$$

The E1-capture involves an integration over angle and is given by

$$(12) \quad \sigma_{p\gamma} = \frac{2k_\gamma}{3\hbar v_i} \{2|\langle \tfrac{1}{2}^+ \| T_1^e \| \tfrac{1}{2}^- \rangle|^2 \}$$

where k_γ is wave number of the outgoing photon, v_i is the velocity of the incoming proton in the center-of-mass, and

$$(13) \quad \langle J_1 \| T_1^e \| J_2 \rangle = (2J_2 + 1)^{\frac{1}{2}} \sum_{n\ell_1 j_1} (2j_1+1)^{\frac{1}{2}} \cdot W(J_2 \ 1 \ I_n j_1; J_1 j_2)$$

$$\cdot \langle n\ell_1 j_1 \| T_1^e \| n\ell_2 j_2 \rangle$$

where J_1, J_2 are the total spin of the core plus nucleon system for the initial and final states, I_n is the spin of the core, and the $W(J_2 \ 1 \ I_n j_1; J_1 j_2)$ are Racah coefficients. The reduced matrix element

$$(14) \qquad \langle n\ell_1 j_1 \| T_1^e \| n\ell_2 j_2 \rangle = i^{\ell_1 - \ell_2 + 1} (-1)^{j_1 - \frac{1}{2}} \frac{(2_{j_2} + 1)^{\frac{1}{2}}}{\sqrt{3}}$$

$$\cdot (j_1 j_2 \tfrac{1}{2} -\tfrac{1}{2} | 10) \, e_{eff} k_\gamma \, OV(n)$$

and
$$OV(n) = \int_o^\infty \frac{\omega_{n\ell_1 j_1}^{J_1 *}}{r} \theta_{E1}(r) \frac{u_{n\ell_2 j_2}^{J_2}}{r} r^2 dr$$

and
$$e_{eff} = \left(\frac{Z_p A_T - Z_T A_p}{A_T + A_p} \right) e$$

where e is the proton charge and (Z_p, A_p), (Z_T, A_T) are the charge and mass number of the projectile and target, respectively, the $(j_1 j_2 \tfrac{1}{2} -\tfrac{1}{2} | 10)$ are Clebsch-Gordan coefficients, $\theta_{E1}(r)$ is the electric dipole operator which reduces to r in the long wavelength approximation, $\omega_{n\ell_1 j_1}^{J_1}$, $u_{n\ell_2 j_2}^{J_2}$ are the <u>nth</u> channel initial and final state wave functions of a nucleon with orbital angular momentum ℓ_2; and total angular momentum j_i, about the core state with total spin I_n to yield a total angular momentum J_i.

The bremsstrahlung differential cross section is multiplied by a density of states to correct for all the continuum final states. This factor consists of two parts: the usual density of momentum in phase space and the area under the final state resonance assuming a Breit-Wigner shape.

The Clebsch-Gordan and Racah coefficients were evaluated using Rotenberg, Bivens, Metropolis, and Wooten, <u>The 3-J and 6-J Symbols</u>, The Technology Press, MIT (1959).

C. NUCLEAR AND COULOMB POTENTIAL SHAPES

The usual diagonal central potential is a Woods-Saxon diffuse edge well form

$$(15) \qquad f = [1 + \exp([R-R_o]/a)]^{-1}$$

where a is a parameter which measures the diffuseness of the edge and R_o is the nuclear radius usually given by $R_o = r_o A^{1/3}$.

The off-diagonal and spin-orbit potential are given in terms of the derivative of the central potential

$$(16) \qquad \frac{df}{dr} = - (\frac{1}{a}) \frac{e^{(R-R_o)/a}}{(1+e^{(R-R_o)/a})^2}$$

The spin-orbit force picks up an additional $1/r$ dependence as presented in Table 1.   The Coulomb potential is the usual uniform sphere value inside the nuclear radius and the standard $1/r$ dependence outside,

$$(17) \qquad V_c(r) = \begin{cases} \dfrac{ZZ'e^2}{2R_o} (3 - \dfrac{r^2}{R_o^2}) & r \leq R_o \\[3mm] \dfrac{ZZ'e^2}{r} & r > R_o \end{cases}$$

D.   COMPUTER PROGRAM INFORMATION

The programs were run on the CDC 7600 high-speed digital computer at Berkeley through the remote terminal in the Downs-Lauritsen physics building. The programs can be contained in two boxes of cards, but testing and production were done using the program storage system at Berkeley. The high speeds and inexpensive costs in running the programs make any timing estimates superfluous.

The linear equation solver package LINIT is a Berkeley computing center program.

All numerical and physical constants values are from F. Ajzenberg-Selone and C. L. Busch, Nuclear "Wallet Cards", University of Pennsylvania, Philadelphia (1971).

REFERENCES

1. E. K. Warburton and J. Weneser, The Role of Isospin in Electromagnetic Transitions, edited by D. H. Wilkinson (North Holland Publishing Company, Amsterdam, 1969), p. 174

2. F. Ajzenberg-Selove, Nucl. Phys. A152 (1970) 1

3. F. Ajzenberg-Selove, Nucl. Phys. A190 (1972) 1

4. P. M. Endt and C. Van der Leun, Nucl. Phys. A214 (1973) 1

5. K. W. Allen, P. G. Lawson, and D. H. Wilkinson, Phys. Lett. 26B (1968) 138

6. S. W. Robinson, C. P. Swann, and V. K. Rasmussen, Phys. Lett. 26B (1968) 298

7. J. D. Seagrave, Phys. Rev. 84 (1951) 1219 and 85 (1952) 197

8. D. F. Hebbard and J. L. Vogl, Nucl. Phys. 21 (1960) 65; W. A. Fowler and J. L. Vogl, Lectures in Theoretical Physics, VI (University of Colorado Press, Boulder, 1964), p. 379

9. F. Riess, P. Paul, J. B. Thomas, and S. S. Hanna, Phys. Rev. 176 (1968) 1140

10. C. Rolfs and R. E. Azuma, Nucl. Phys. A227 (1974) 291

11. D. F. Measday, A. B. Clegg, and P. S. Fisher, Nucl. Phys. 61 (1965) 269

12. J. B. Marion, P. H. Nettles, C. L. Cocke, and G. J. Stephenson, Phys. Rev. 157 (1967) 847

13. I. M. Gel'fand, G. E. Shilov, Generalized Functions, Vol. I (Academic Press, New York, 1964).

14. T. Tamura, Rev. Mod. Phys. 37 (1965) 679

15. D. L. Johnson, thesis, University of Washington (1974) unpublished

16. H. J. Rose and D. M. Brink, Rev. Mod. Phys. 39 (1967) 306

17. Abramowitz and Stegin, Handbook of Mathematical Functions (1964)

18. S. Cohen and D. Kurath, Nucl. Phys. 73 (1965) 1; Nucl. Phys. A101 (1967) 1

19. O. Mikoshiba, T. Terasawa, and M. Tanifuji, Nucl. Phys. A168 (1971) 417

20. H. L. Jackson and A. I. Galonsky, Phys. Rev. 89 (1953) 370

21. D. Kurath, submitted to Phys. Rev. Comments (1975)

22. M. D. Melkanoff, T. Saweda, J. Raynal, Methods in Computational Physics, Vol. 6 (Academic Press, New York, 1967)

23. A. H. Stroud and Don Secrest, Gaussian Quadrature Formulas (Prentice Hall, Englewood Cliffs, N. J., 1966)

TABLE 1

		WIDTHS	
		THEORY	EXPERIMENTAL
$1/2+ \rightarrow 1/2^-$	$\Gamma_\gamma(^{13}C)$	.617 eV	.44 ± .05 eV
	$\Gamma_\gamma(^{13}N)$	.701 eV	.64 ± .07 eV
	Ratio of Strengths	2.52	3.2 ± 0.7
$3/2^- \rightarrow 1/2^+$	$\Gamma_\gamma(^{13}C)$	2.5 meV	6.6 meV
	$\Gamma_\gamma(^{13}N)$	4.2 meV	4.4 meV
	Ratio of Strengths	.240	.095

It should be noted that the $3/2^-$ to $1/2^+$ transition widths are in millielectron volts (10^{-3} eV). In this transition strong interference between channels yields a large error in the theoretical width values.

TABLE 2

STATE	MIXING	POTENTIALS SPIN—ORBIT	CENTRAL (MeV)	SPECTROSCOPIC FACTORS
^{13}C(g.s.)	2.22	.93	40.207	(.8252, 1.6091)
^{13}N(g.s.)	2.22	.93	40.257	(.8812, 1.5531)
^{13}C(1/2+)	2.73	.31	53.304	(.905, .095)
^{13}N(1/2+)	2.73	.31	54.263	(.922, .078)
^{13}C(3/2$^-$)	1.6	0.	42.557	(.142, .858)
^{13}N(3/2$^-$)	1.6	0.	43.355	(.136, .864)

The full mixing potential is a product of the factor given above times $(hc/2mc^2)$, the Compton wave length of the reduced mass, times the derivative of the central Woods-Saxon form. Similarly the spin-orbit potential is a product of the above factor times $(h^2c^2/2mc^2)$ times $(\vec{\sigma}\cdot\vec{L})/r$ times the derivative of the Woods-Saxon form. The matching radius is 22.35 fm. The mixing strength corresponds to a rotational model with $\beta=-1/2$.

Figure 1. Ratio of corresponding E1 strengths in light mirror nuclei. The data have been obtained from the data compilations of refs. 2-4. The indicated ratio for A = 15 is an upper limit.

E1-STRENGTHS IN MIRROR NUCLEI

EXPECTED RATIO

A = 13
(E1~0.1 W.u.)

A = 17-43
(E1~10⁻³-10⁻⁶ W.u.)

A = 15
(E1~10⁻⁶ W.u.)

NUMBER OF EXAMPLES

RATIO OF E1-STRENGTHS
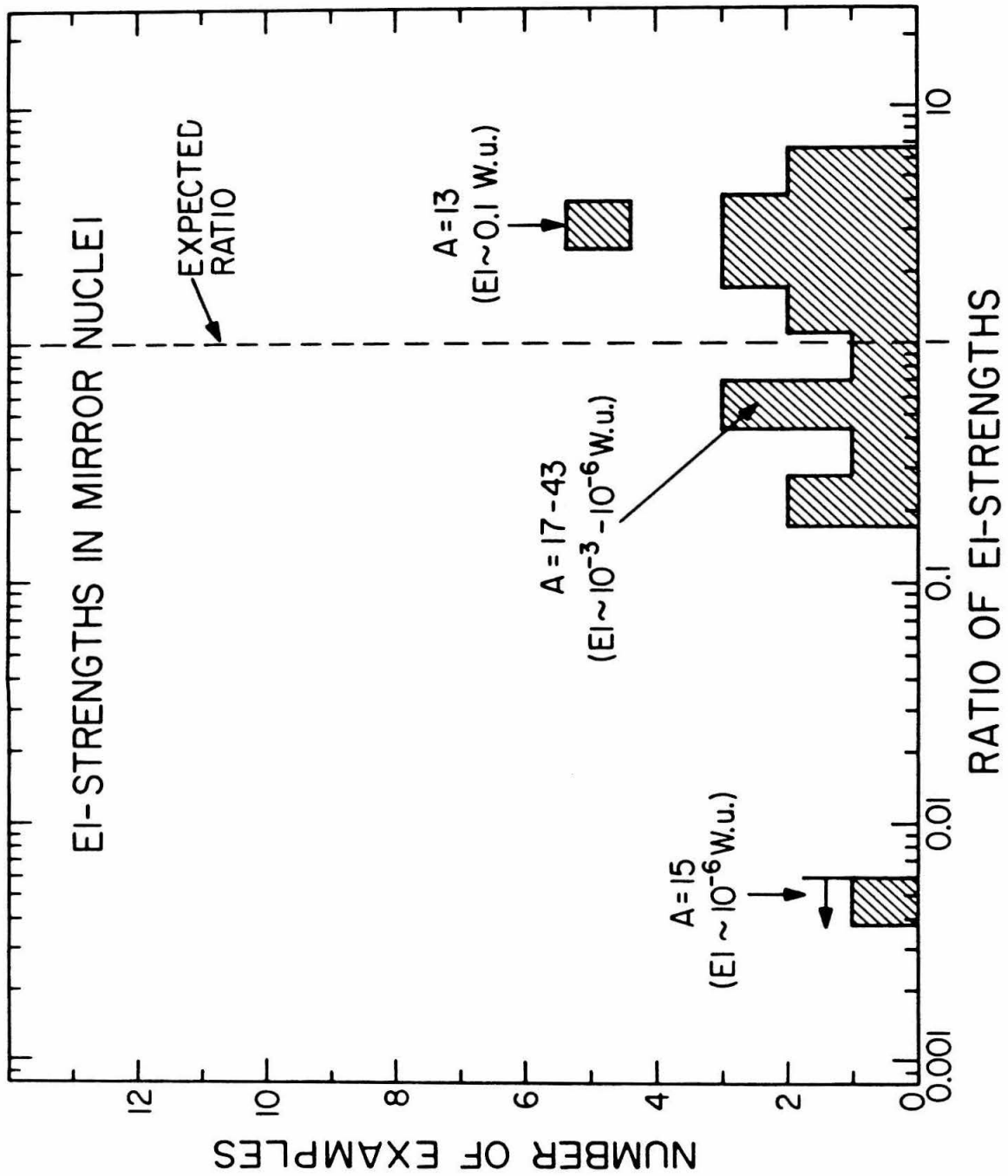
Figure 2.   Isobar energy level diagram for A = 13.

Note that no correction is made for the Coulomb energy difference between ^{13}C and ^{13}N.

ISOBAR DIAGRAM A = 13

2$^+$ 4.439

6.898 3/2$^+$

6.382 5/2$^+$ 4.439   2$^+$

6.864 5/2$^+$

O$^+$

(4.947)

^{12}C + n

3.547 5/2$^+$

3.509 3/2$^-$

2.366 1/2$^+$

3.854 5/2$^+$

3.684 3/2$^-$

3.086 1/2$^+$

O$^+$

(1.944)

^{12}C + p

1/2$^-$

2m$_0$c^2 (2.221)

^{13}N

1/2$^-$

^{13}C
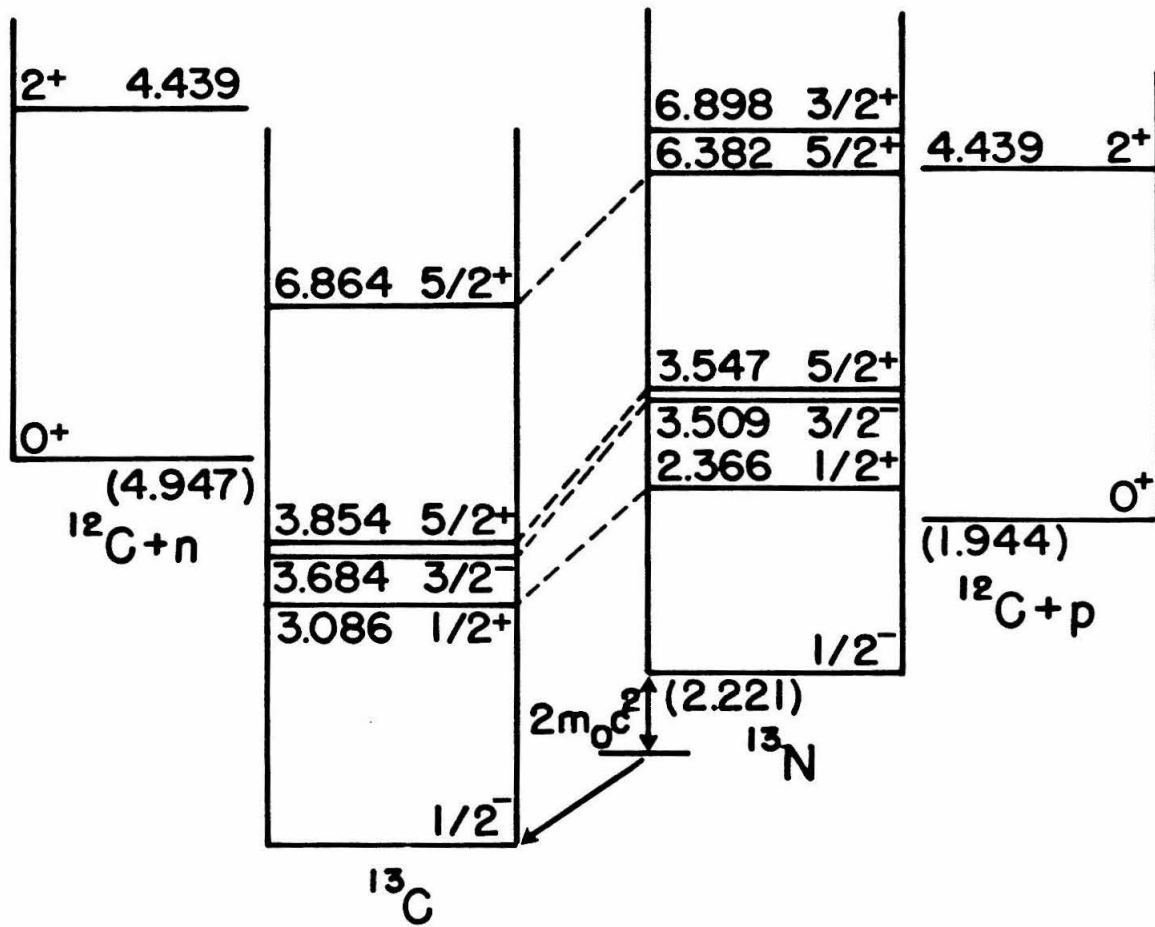
Figure 3. Comparison of the experimental $S_{1/2}$ phase shifts with the model calculations for the $^{12}C(p,p)^{12}C$ reaction. The data are taken from ref. 20.

$^{12}C(p,p)^{12}C$

PHASE SHIFT δ_0

PROTON ENERGY (keV)
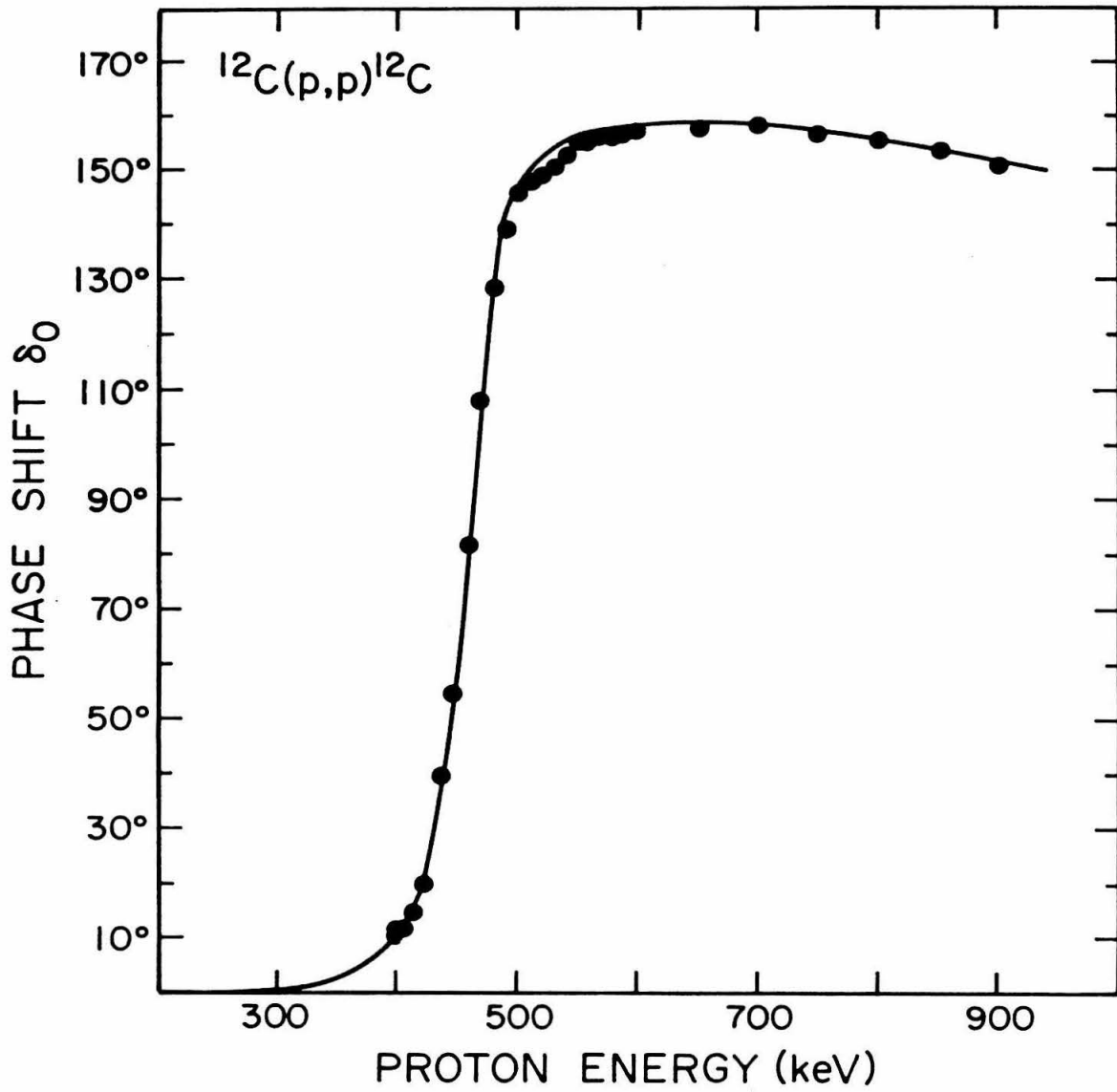
Figure 4. Capture cross section near the resonance peak.
Dots are data of Rolfs[10]. The solid curve is the theoretical fit.

$^{12}C(p,\gamma)^{13}N$
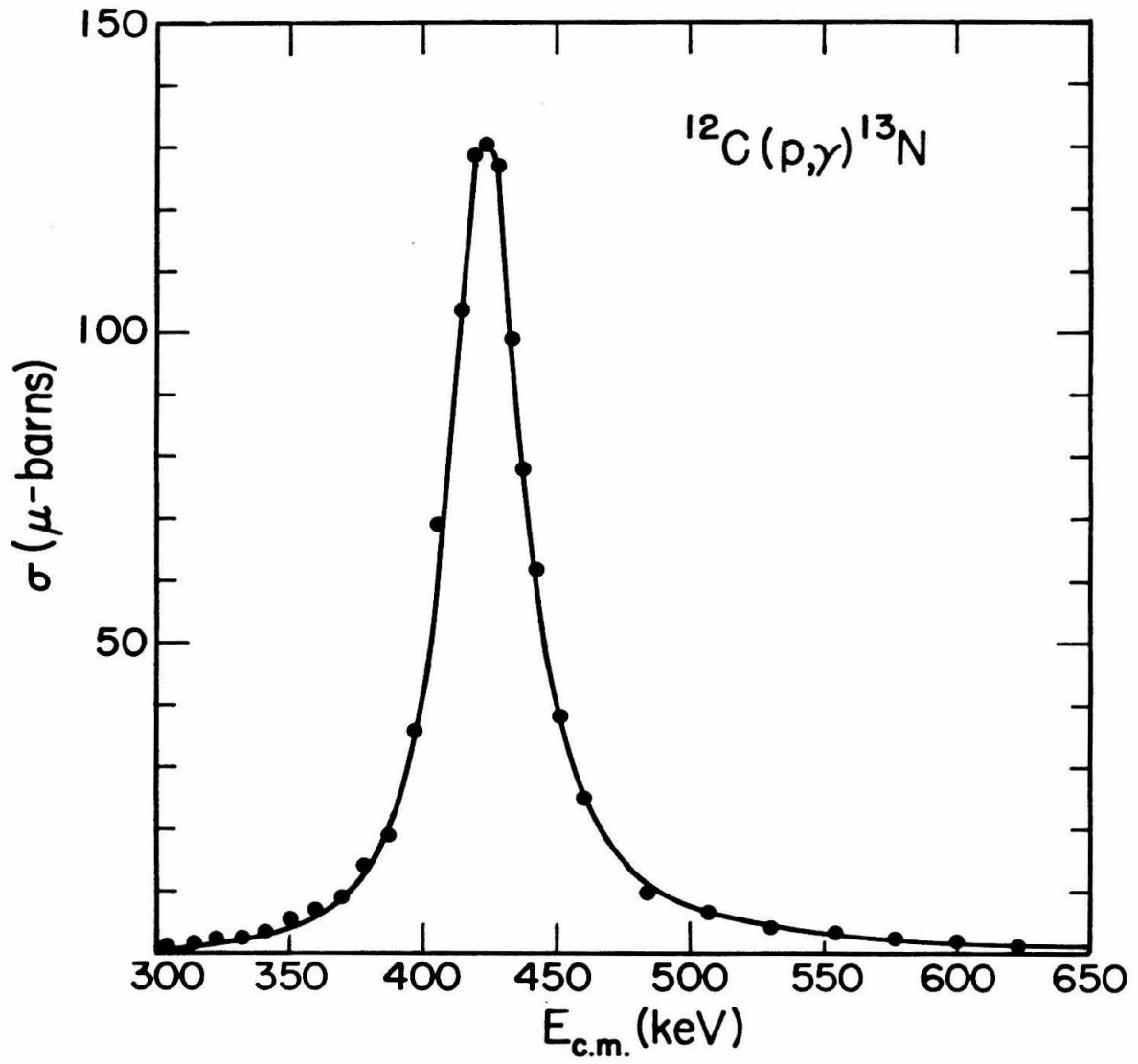
Figure 5.   S-factor given by $S = \sigma E \exp(2\pi\eta)$.

Solid curve is theoretical fit. The circles are the data of Rolfs[10]. The plus signs are the data of Vogl[8]. The dashed curve is a single channel fit with no mixing.

$^{12}C(p, \gamma)^{13}N$

● Rolfs data
+ Vogl data

S (keV-barns)

E_{CM} (keV)
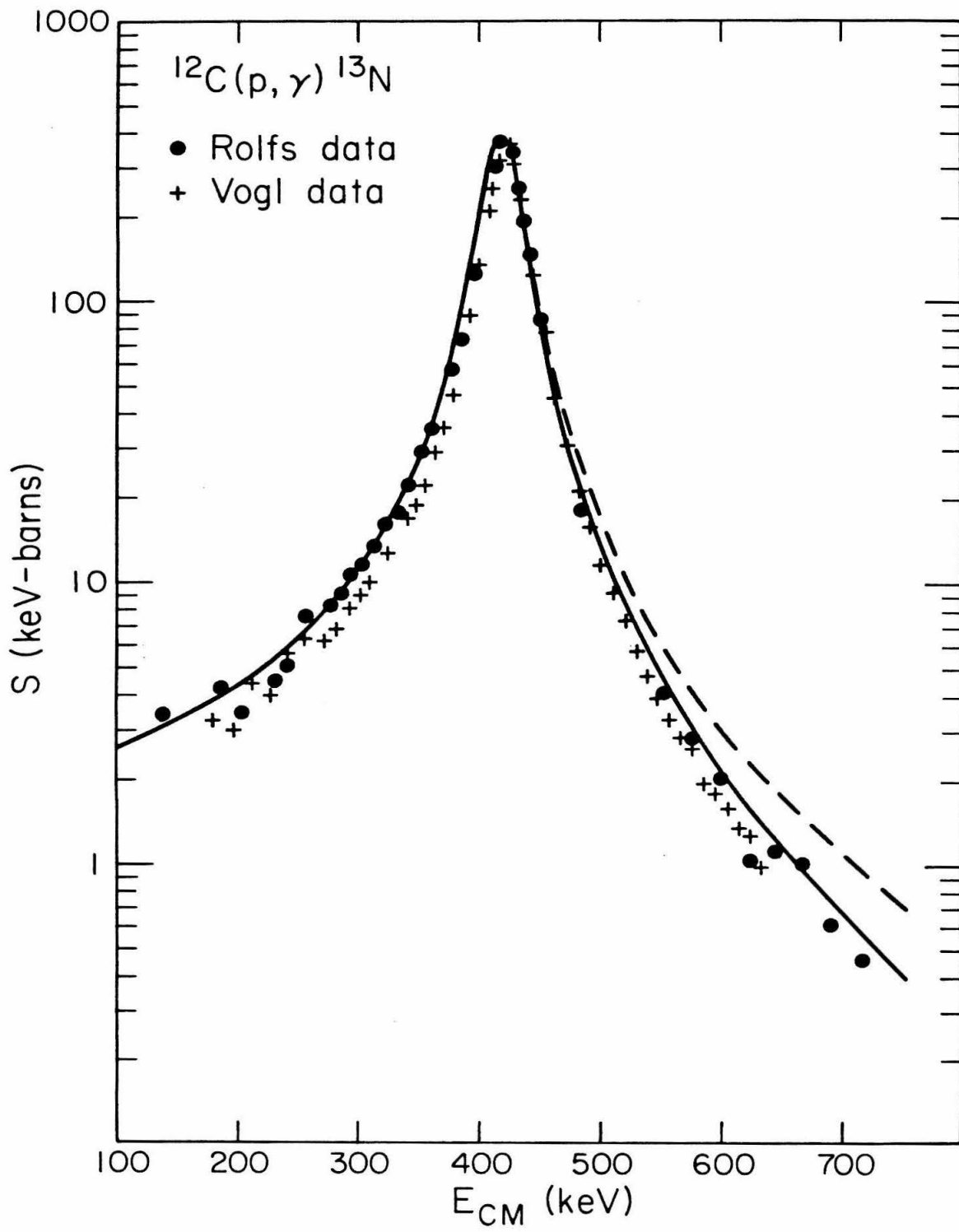
Figure 6. Differential cross sections for bremsstrahlung at 0° and 90°.
The data are from Rolfs[10]. The dashed curve is the preliminary fit
using a Breit-Wigner form to represent line shape. The solid
curves are the result of integration over the calculated line
shape.

$^{12}C(p, \gamma p^*)^{12}C$
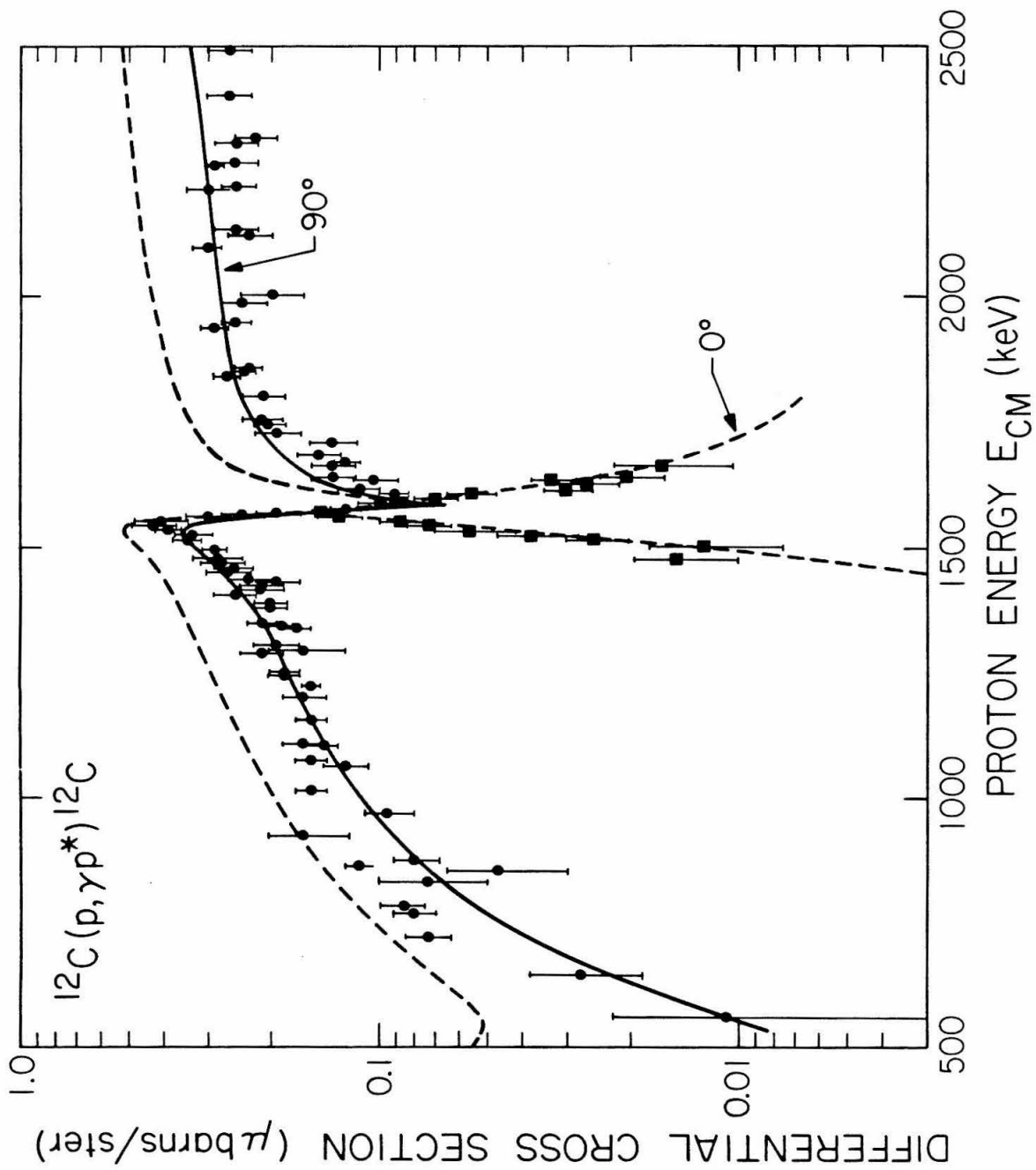
Figure 7. The gamma ray line shapes for bremsstrahlung at 90°. The dashed lines are the lower limits for integration over the peaks.